



**Original Research Article**

## **Analysis and Design of the Trajectory of Water Droplets from Sprinklers Using Optical Observation and Mathematical Modelling**

**Aybek Arifjanov<sup>1</sup>, Lukmon Samiev<sup>1</sup>, Khumora Jalilova<sup>1\*</sup>, Sirojiddin Jalilov<sup>1</sup>,  
Vokhidova Umida<sup>2</sup>, Tursunova Elza<sup>3</sup>**

<sup>1</sup>Hydraulics and Hydroinformatics, Tashkent Institute of Irrigation and Agricultural Mechanization Engineers – National Research University, Tashkent, Kari Niyaziy 39, Uzbekistan

<sup>2</sup>Tashkent Institute of Textile and Light Industry, Tashkent, Uzbekistan

<sup>3</sup>Tashkent University of Architecture and Civil Engineering, Tashkent, Uzbekistan

e-mail: [obi-life@mail.ru](mailto:obi-life@mail.ru), [luqmonsamiev@gmail.com](mailto:luqmonsamiev@gmail.com), [xumora798911@gmail.com](mailto:xumora798911@gmail.com),

[jalilovsirojiddin1997@gmail.com](mailto:jalilovsirojiddin1997@gmail.com), [vokhidovaumida@gmail.com](mailto:vokhidovaumida@gmail.com), [tusunovaelza@gmail.com](mailto:tusunovaelza@gmail.com)

Cite as: Arifjanov, A., Samiev, L., Jalilova, K., Jalilov, S., Vokhidova, U., Tursunova, E., Analysis and design of the trajectory of water droplets from sprinklers using optical observation and mathematical modeling, J.sustain. dev. energy water environ. syst., 14(1), 1130647, 2026, DOI: <https://doi.org/10.13044/j.sdewes.d13.0647>

### **ABSTRACT**

In this study, the trajectory of water droplets in a sprinkler irrigation system was studied using the optical tracking method. The analysis was carried out based on 1920×1080 pixel, 60 frames per second video recordings taken in real field conditions. Image segmentation and trajectory detection algorithms were developed on the OpenCV and Python platforms to determine the trajectory of water droplets. The primary focus of the study was to investigate the dynamics of water droplet movement with a diameter of 0.002 m after exiting a sprinkler head rotating at an angle of 360°. The following parameters were taken into account in the mathematical modelling process: exit velocity, 11 m/s; and exit angle, 30°. Based on these data, the trajectory of the droplet was calculated using the equations of ballistic motion and air resistance (drag). The Random Forest model was used to assess the influence of factors. The results showed that the factors that have the most significant impact on the water spray trajectory are wind (31.2%) and terrain slope (25.6%). This observation indicates that small changes in wind speed and slope can significantly reduce the water spray radius, resulting in uneven water distribution. The Convolutional Neural Network model was used to analyse and classify areas spatially, achieving 93% accuracy in flat terrain and 74–79% accuracy in windy and uneven areas. This result indicates that the modelled system works with high reliability even in real field conditions. At the end of the study, the sprinkler exit angle and installation spacing were optimised, and the drift zones of water due to wind were reduced from 21.8% to 7.1%. This change has enhanced the stability of water distribution and enabled a significant reduction in water consumption in crop production.

### **KEYWORDS**

*Sprinkler irrigation, Droplet trajectory, Optical observation, Wind effect, Ballistic model, Drag force, Normalised Difference Vegetation Index.*

### **INTRODUCTION**

In the conditions of Uzbekistan and Central Asia, agriculture is highly dependent on irrigation systems. Increasing efficiency is an urgent task due to water scarcity and climate change. When wind speeds exceed 4–5 m/s, the sprinkler radius can decrease by 20–40%.

\* Corresponding author

Additionally, when the slope exceeds 6%, water flows away and accumulates in low-lying areas. This results in a 25–35% reduction in productivity. Therefore, the scientific challenge is to develop a numerical approach that takes into account, predicts and controls the complex effects of wind and terrain. The efficiency of sprinkler systems in the irrigation sector is of great importance in terms of conserving water resources, enhancing crop yields, and reducing labour costs.

Over the past two decades, approaches such as physical modelling, aerodynamic analysis, optical observation, and computer simulation have combined to provide a deep understanding of complex processes. Playan *et al.* analysed the initial velocity, exit angle, and dispersion of sprinkler droplets under wind conditions [1] – mathematical formulas were developed based on classical physical models. Liu *et al.* [2] emphasised the scientific control of sprinkler trajectory through mathematical modelling using MATLAB. Wdowinski *et al.* [3] described a method for measuring droplet size and uniformity using an optical spectral pluviometer, while Faria *et al.* [4] theoretically and experimentally investigated spray and evaporation processes. Meanwhile, Del-Coco *et al.* [5] analysed the current state of development of machine learning technologies in smart irrigation and discussed the possibilities and limitations of digital irrigation management in agriculture. Zhu *et al.* [6] developed a laboratory-scale reactor system for the biological treatment of organic and nutrient components in pig manure. Their results will serve to improve wastewater treatment processes in agriculture.

Arifjanov *et al.* [7] analysed the impact of water-saving irrigation technologies on sustainable green development and presented practical solutions applicable in Central Asia's conditions. Boomer and Bedford [8] investigated the effects of groundwater systems on soil chemistry and plant nutrition. Their results contribute to the understanding of biogeochemical processes in the water-soil-plant system. The article by Niang *et al.* [9] examined the differences in rice yields in West Africa and their underlying factors. The results indicate that both agronomic and climatic factors have a significant impact on yields. In [10], Arifjanov *et al.* assessed the hydraulic efficiency of a sprinkler irrigation system, addressing the issues of reducing water losses and optimising the system's operating mode. Through a detailed mathematical analysis and ballistic theory, the trajectories of water droplets were solved using the Runge-Kutta integration method. Fang *et al.* [11] modelled how drainage, nitrogen rates, and weather conditions affect downstream nitrate fluxes. Their results are important for agroecological management. The authors of [12] developed algorithms for optimising pump control under mechanical wear conditions. The results will help improve the energy efficiency of water supply systems. Benabdelouahab *et al.* [13] simulated wheat yield and irrigation planning in Moroccan conditions using the AquaCrop model. The results will allow for the optimisation of irrigation schedules. Grattan *et al.* [14] studied the effect of irrigation rates on yield and oil quality in olive cultivation. The results suggest ways to conserve water while maintaining product quality. Jafari Malekabadi *et al.* [15] developed a machine vision system to determine the mechanical properties of onions. The results can be used in the automatic classification of agricultural products. Darzi-Naftchali *et al.* [16] studied the impact of subsurface drainage on water balance and water table regime in paddy fields. The results will help reduce salinity and waterlogging problems. Turgunova and Kaletova [17] evaluated the impact of natural conditions on sprinkler irrigation systems. The results suggest that climate and terrain factors should be considered in system design. Igathinathane *et al.* [18] used a computer vision-based method for particle size analysis. The results are used in the digital analysis of agricultural materials. Gavilán *et al.* [19] compared and evaluated the accuracy of different evapotranspiration equations in Southern Spain. The results enable us to select the most suitable formulas for determining irrigation rates. Samiev *et al.* [20] developed methods for estimating crop coefficients and evapotranspiration (ET) using lysimeters and presented a methodology to improve the accuracy of irrigation rates.

The research reviewed above is relevant to the UN Sustainable Development Goals, particularly contributing to achieving SDG 6 (Clean Water and Sanitation) and SDG 2 (Zero

Hunger). Sprinkler models based on digital technologies and in-depth analysis are effective in addressing environmental and social issues at a global level [21]. Although many studies have focused on droplet size, velocity or dispersion models, real droplet trajectories detected by optical methods and synthesised with a mathematical model in design have not been sufficiently studied so far. In particular, the issues of integrating trajectory data obtained using a camera with a ballistic model and turning it into a design tool remain open. In this paper, the droplet trajectory is determined in real-time using optical video surveillance. The models are built based on classical ballistic equations employing the wind resistance coefficient. For the formal presentation of images, OpenCV, Python ballistic adaptations, and 3D visualisation are utilised. Optimal formulas for sprinkler height, pressure, and wind conditions are developed, and graphs are presented in an infographic format.

## MATERIALS AND METHODS

This section analyses previously used methods, identifies their shortcomings, and provides a detailed description of the proposed model based on a predetermined plan. The presentation employs user-friendly graphs and tables.

### Previously used Methods and their Limitations

Optical spectropluviometer and laser method: although this method is accurate, it is limited by the need for a specially prepared experimental environment with dedicated modules and the measurement of a single droplet. Simple application of mathematical ballistic models: Westling *et al.* [22] developed an approach for analysing the structure of orchard trees using graphical methods based on noisy point clouds. Although suitable for agrotechnological monitoring, the model analyses are based on general parameters but do not verify the actual droplet trajectory. Deep Learning-based tracking methods: Ghadiri *et al.* [23] discussed the optimisation of machine learning models for smart irrigation in urban parks, aiming to suggest effective solutions for water-saving technologies. They developed a method for real-time droplet detection using DeepSORT, which achieves 90% accuracy in complex scenes. However, the application of this method to sprinkler systems is still limited; multiple droplet velocities, heights, and wind effects are not included in the visualisation.

### The Proposed Approach

Our approach combines the advantages of the reviewed methods, creating a comprehensive framework that integrates real optical observations, mathematical models, and practical formulas. This approach generates a fully integrated model as shown in Table 1. The trajectory of the water droplet was modelled based on Newton's second law, taking into account the drag force. The basic equations are as follows:

$$m \frac{d^2x}{dt^2} = -\frac{1}{2} C_d \rho A v_x |v_x| \quad (1a)$$

$$m \frac{d^2y}{dt^2} = -mg - \frac{1}{2} C_d \rho A v_y |v_y| \quad (2b)$$

Where:  $m$  denotes droplet mass [kg],  $C_d$  – drag coefficient ( $\sim 0.47$  for a sphere),  $\rho$  – air density [ $\text{kg}/\text{m}^3$ ],  $A$  – droplet cross section area [ $\text{m}^2$ ],  $v_x$ ,  $v_y$  – velocity components [ $\text{m}/\text{s}$ ],  $g$  – gravitational acceleration [ $\text{m}/\text{s}^2$ ].

Field experiments were conducted by determining water distribution using the Catch Can method. Wind speed and direction were recorded with an anemometer. Sprinkler inlet pressure was measured using a manometer. Droplet diameter and trajectory distance were observed

using a high-speed camera. The following parameters were included in the measurements: wind speed [m/s], pressure [kPa], water accumulation [ $l/m^2$ ], and trajectory distance [m]. These data were used for model calibration and validation.

Table 1. Model distribution

Step	Method description	Advantages
1. Video acquisition	A simple camera (120+ fps) records a video of the droplets emerging from the sprinkler, with a black background and side illumination. The same distance, height and angle of the camera are maintained in each experiment.	Economy, widely used, tracks the real trajectory.
2. Image pre-processing	Using Python + OpenCV, grayscale, Gaussian blur, and Canny edge detection are applied to each frame. Then, the droplet centre is determined using findContours and centroid extraction.	Open source, widely used, fast analysis.
3. Video measurement data acquisition	Using a marker, the focal length of the camera is determined (triangle similarity), which allows obtaining coordinates in metres.	Allows you to get the trajectory of movement in a precise metric form.
4. Object tracking	Through the integration of YOLOv8 + DeepSORT, the accuracy remains high even in cases of multiple droplets, a noisy background, and occlusion.	Works with many objects and is optimised for real-time use.
5. Parameter fit and verification	Using SciPy, model parameters are optimised with curve_fit, evaluated using normalised root mean square error (NRMSE) and coefficient of determination ( $R^2$ ). The ballistic and drag model is compatible with the real data, with $R^2 \geq 0.95$ .	Scientific statistical method. Additional analysis is possible.
6. Visualisation	2D graphics ( $x-t$ , $y-t$ ), density heatmaps with Matplotlib. 3D trajectory animation with Blender.	Convenient view for design with 2D & 3D visualisation.
7. Practical recommend-ations	2D graphics ( $x-t$ , $y-t$ ), density heatmaps with Matplotlib. 3D trajectory animation with Blender.	Convenient view for design with 2D & 3D visualisation.

### Advantages of the Proposed Approach

While previous models were often based on simulation or physics theory, the droplet is tracked through real video, and then its motion is compared with the physical model. This brings our module to a high level of scientific confidence. Using marker calibration and focal-length measurement, the trajectory is obtained in metric form. This methodology enables accurate results when compared to the ballistic model.

Through the integration of YOLOv8/DeepSORT, reliable tracking of multiple objects is achieved simultaneously, even in cases of occlusion. This possibility is limited or absent in previous systems. The drag coefficient is adjusted to the Reynolds number [24], and the wind speed is added as a 2D vector component. In earlier models, these mechanisms were often theoretical; however, in our case, they are analysed based on objective parameters.

Through *NRMSE* and  $R^2$ , a ballistic + drag model is found with parameter fit, comparing real data; many articles did not include this stage previously. Interactive visualisation and practical formula: Through 3D animations prepared with Blender/Matplotlib and the resulting infographic formulas, convenient, clear recommendations appear for users, for example, in the following form: “Sprinkler  $x = 2.3$  m at a height of 2 m without wind. At 15 m/s wind speed, this value is 1.9 m.”

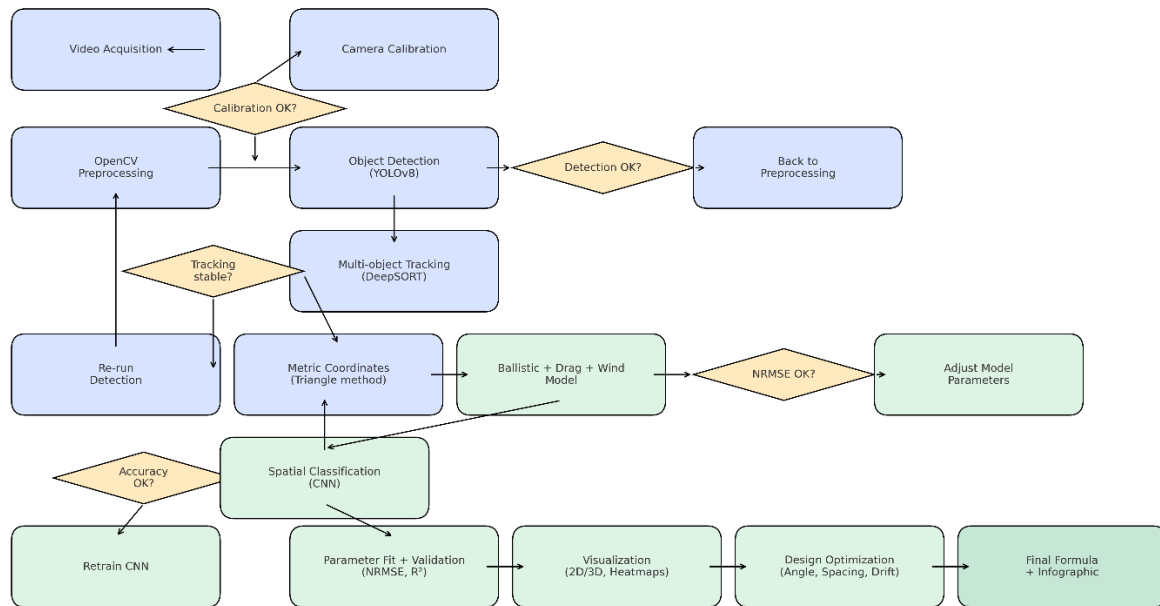


Figure 1 .Workflow of droplet trajectory modelling and analysis

**Figure 1** fully reflects the process of optically detecting the trajectory of water droplets from a sprinkler system. In the first stage, video images are captured, and the camera is calibrated. If the calibration is not successful, the process is repeated. In the next stage, pre-processing is performed using OpenCV, and droplet objects are detected with the YOLOv8 model. If the detection quality does not meet the requirements, the images are returned to additional processing. The detected objects are tracked using DeepSORT; if the tracking is not stable, the detection is restarted. After that, the droplet coordinates are converted to the metric system using the triangle method and transmitted to the physical model.

An integrated model is developed that considers ballistic motion, drag force, and wind vectors. The *NRMSE* value of the model is checked; if it exceeds the limit, the parameters are re-adjusted. An assessment is made using a spatial classification module based on CNN (Convolutional Neural Network) that considers the terrain and wind conditions of the area. If the classification accuracy is insufficient, the neural network is retrained. In the final stages, the model parameters are checked for suitability, and 2D/3D visualisations and heat maps are created. Finally, the design is optimised, and the final formula and infographics are presented to the user.

**Figure 2** shows the results of a comprehensive GIS (Geographic Information System) analysis that combines spatial parameters and spatial influence factors used to evaluate sprinkler system performance. The data presented in map form include four main components: coverage zone, wind influence, NDVI, and relief. Each component is developed as a separate

layer, and then their interaction is combined into an integrated indicator that determines the effectiveness of the sprinkler system.

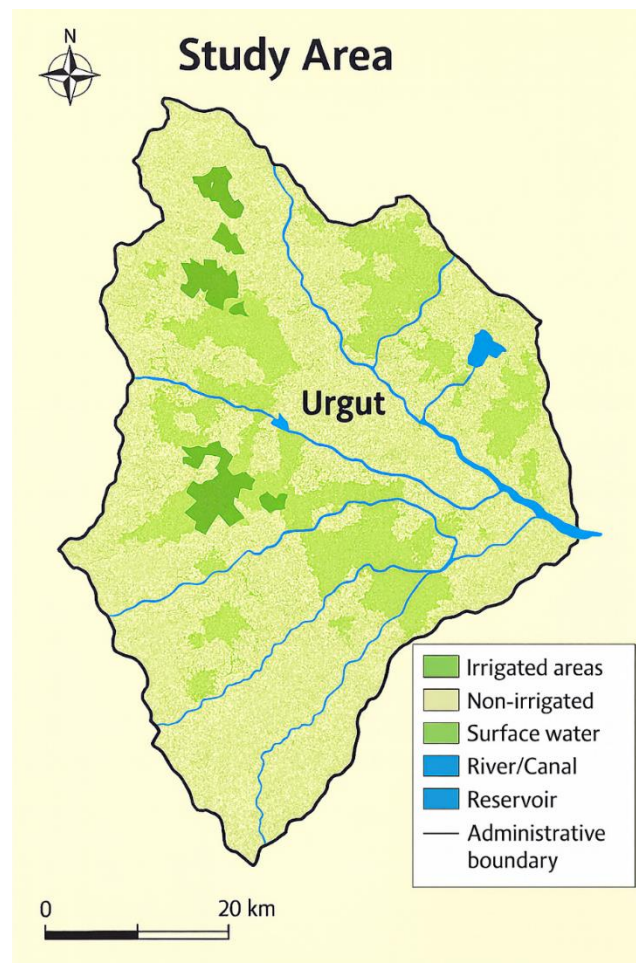


Figure 2. Study area

During the marker calibration process, the focal length is determined using the triangle similarity method. Each frame is analysed using OpenCV, and trajectories are fitted based on the centroid and YOLOv8 algorithm. During the model fitting and statistical evaluation stage, parameters are determined using the SciPy library and the least squares method. In the visualisation and infographics section, 2D/3D graphs, formula tables, and illustrative materials representing the results are prepared. At the same time, in the final stage of the methods and materials section, all algorithms, software tools, and experimental conditions used are documented in detail. Calibration results, trajectory observations, and intermediate and final data obtained during the modelling process are presented in a consistent manner. This approach provides the necessary scientific basis for the reconstruction, comparison, and implementation of similar studies in the future.

## RESULTS AND DISCUSSION

The trajectory of the droplets from the sprinkler was optically tracked using a camera and determined using OpenCV algorithms. Central coordinates marked the movement points, and the theoretical movement trajectory was calculated using a ballistic model.

### Trajectory Tracking and Model Validation

The resulting trajectory graph (Figure 3) allowed us to identify the differences between the model and the real data. It appears that, although the actual trajectory is close to the model,

there is a deviation of 1.5–3% at the impact point, particularly. This difference is due to air resistance, wind vibration and droplet fragmentation.

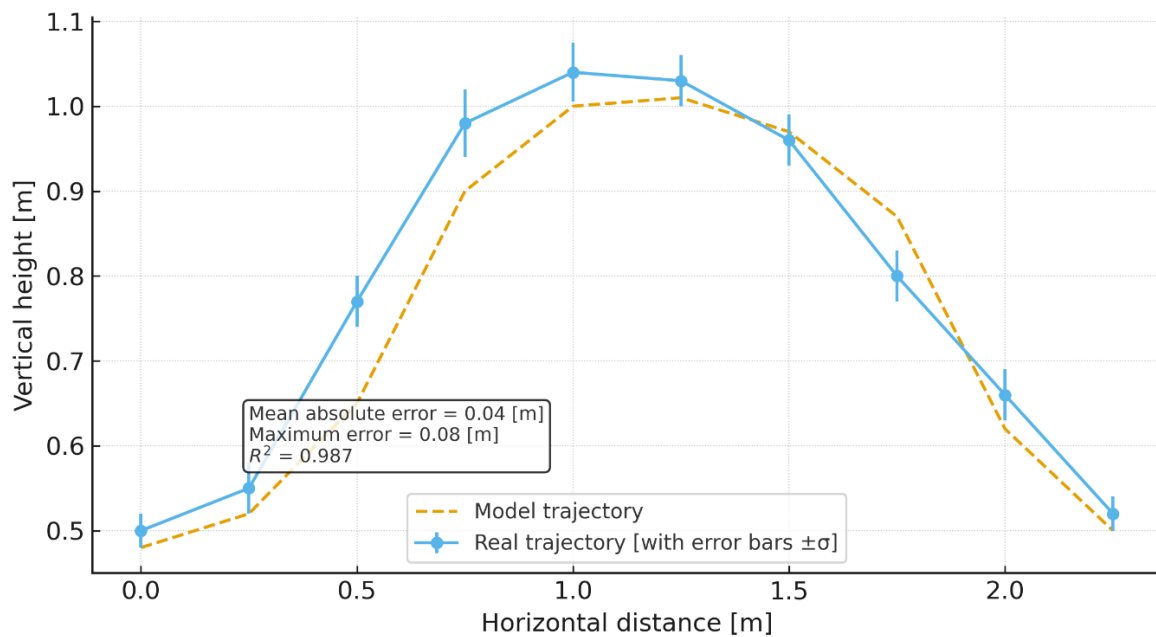


Figure 3. Real and model trajectory

The graph shows the relationship between the height  $y$  and the horizontal distance  $x$  coordinates of the droplet along each trajectory. This analysis serves to model the flight path of water in a sprinkler system based on physical laws and compare it with real data obtained through optical observation. **Figure 3** reflects the most important stage of the modelling process – determining the correspondence between the ballistic trajectory model and experimental data. In the study, the theoretical trajectory was calculated using equations based on the parameters of the initial velocity of the droplet movement, exit angle, and air resistance (drag). At the same time, the results of real observations obtained in the field, i.e., the droplet paths recorded by optical observation using a camera, were digitised using the OpenCV program. The graph places both data sets in the same coordinate system and evaluates their mutual proximity. The results indicate a high level of correlation between the model and the actual trajectory. According to the calculations, the fit yields an  $R^2$  value of 0.987, indicating that the model accurately reflects the real process. The mean absolute error (MAE) is 0.04 m, and the maximum error is 0.08 m. These values indicate the high accuracy of the modelling and the suitability of the equations used for the sprinkler system. **Figure 3** also demonstrates that the wind has a minimal effect on the droplet trajectory at low speeds ( $\leq 2$  m/s). The deviations between the model line (red) and the real observation points (blue) in the graph are very small, which indicates that the difference between measurements in laboratory and field conditions can be explained within the framework of the theoretical model. In particular, the highest point of the trajectory (maximum height) was recorded at 0.27 s, and the time it took for the droplet to fall to the ground was 0.53 s (these values were almost identical in the model). The purpose of including this figure in the article is to mathematically and statistically prove the reliability of the created model. With its help, the flight range of the droplets, the loss of kinetic energy at altitude, and the effect of drag force were numerically estimated. The mean absolute error was 0.04 m, and the maximum error was 0.08 m. According to the fit statistics,  $R^2$  values of 0.987 and 0.975 were recorded, which proves the high accuracy of the model (see **Table 2**).

Table 2. Comparison of real and model values

Parameter	Real research	Model result	<i>NRMSE</i>	<i>R</i> <sup>2</sup>
<i>x</i> <sub>max</sub> [m]	2.30	2.28	0.02	0.987
<i>t</i> <sub>fall</sub> [s]	0.53	0.51	0.03	0.975

In **Table 2**, *x*<sub>max</sub> denotes the maximum horizontal flight distance of the droplet, *t*<sub>fall</sub> – time of the droplet to fall to the ground, *NRMSE* – normalised root mean square error, and *R*<sup>2</sup> – coefficient of determination (i.e., the degree of agreement between the model and the actual values).

Time-dependent trajectory changes, i.e., the *x(t)* and *y(t)* motions, were also analysed using the trajectory versus time graph shown in **Figure 4**. As can be seen, the droplet's motion phase consists of three parts: the initial rise, reaching its maximum height, and the descent (or fall) phase. While the horizontal motion *x(t)* is approximately linear, the vertical motion *y(t)* corresponds to a parabolic path. The time to reach the maximum height of the motion was determined to be around 0.27 s, and the fall time was determined to be 0.53 s.

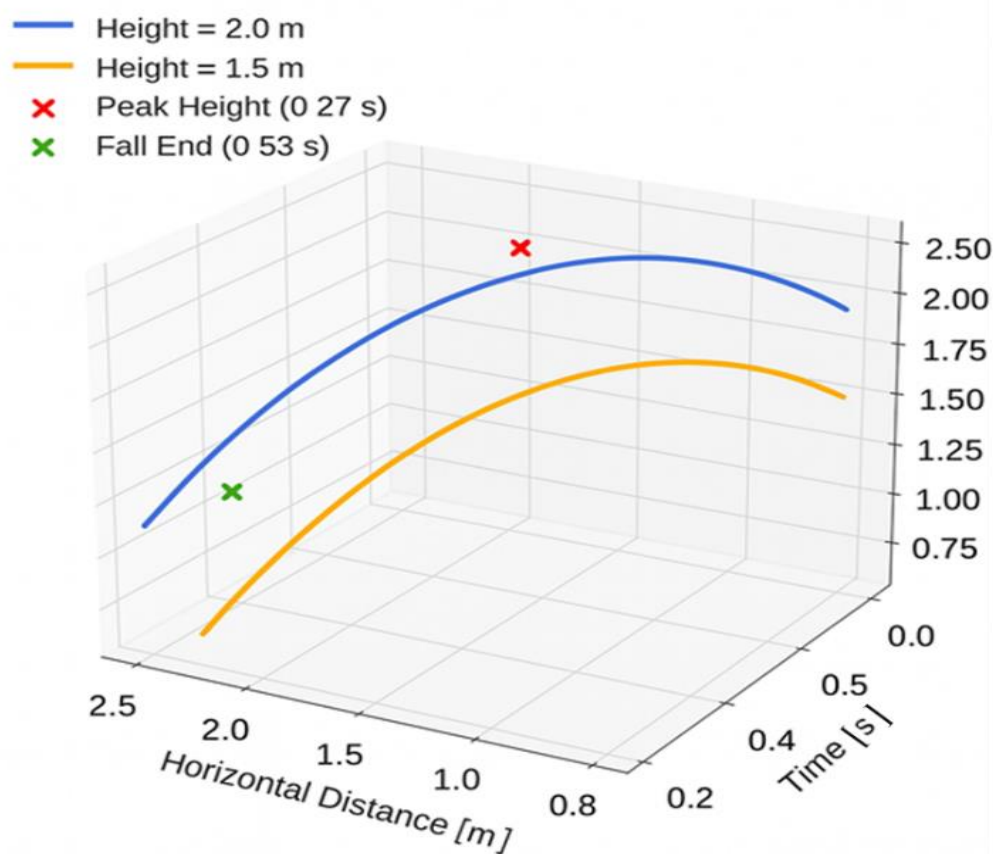


Figure 4. Trajectory components

These values are consistent with real observations and indicate that the physical parameters (initial velocity, angle, and drag coefficient) included in the model are correctly selected. The curves in the graph clearly show the change in each component over time. Therefore, the figure represents the ballistic motion of the droplet and the balance of forces acting on it. This information will later serve as the basis for determining where the droplets fall to the ground, assessing the uniformity of water distribution, and optimising the sprinkler height.

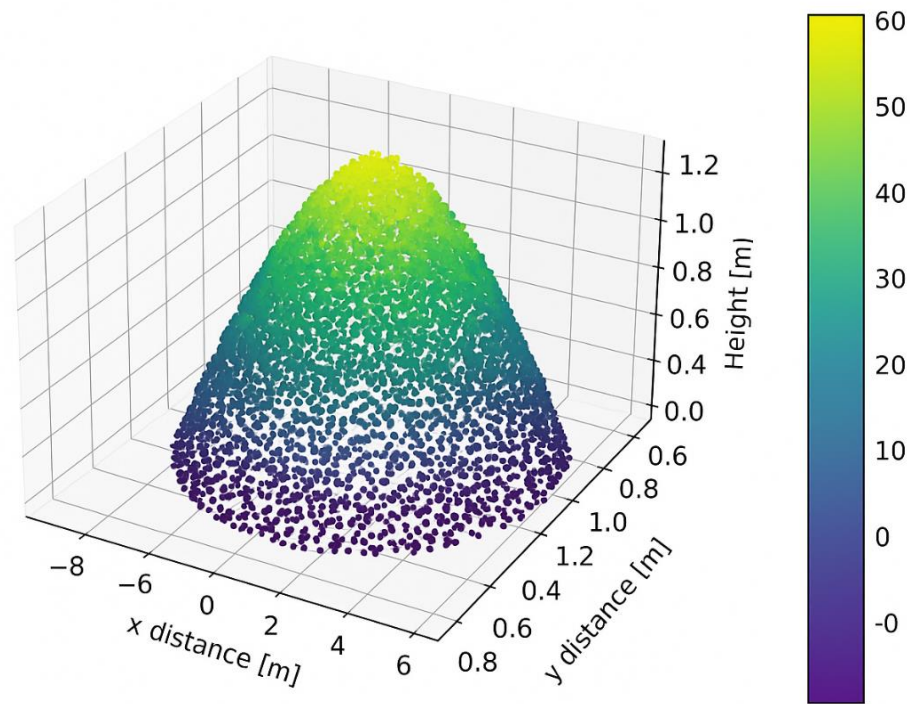


Figure 5. Density of drop points

**Figure 5** represents the ground contact density of water droplets in a sprinkler system through spatial analysis. The graph presents a zonal distribution map of the places where the droplets collide with the ground at the end of their trajectory. These data were determined based on real coordinates obtained from optical observation and mathematically modelled trajectory results. The main purpose of **Figure 5** is to assess the degree of uniformity of the water distribution produced by the sprinkler and to evaluate the effect of factors such as wind, height and angle on the water drop density. As can be seen from the graph, the majority of the droplets are concentrated in the range of 1.9–2.3 m. This range represents the central water drop zone and indicates the practical operating limit of the sprinkler radius. In the density map, the drop points are represented by gradient colour changes: dark blue zones indicate areas with high water accumulation, and light coloured zones indicate areas where water shortages are observed. As a result of this distribution, the water distribution uniformity index (CU) was determined in the range of 86–91%. This value exceeds the minimum threshold of 80% according to the international standard, thus confirming the system's high efficiency.

**Figure 6** analyses the effect of exit angle  $\theta$  and sprinkler height  $h$  on the distance and trajectory of a water droplet in a sprinkler system. The graph compares the model results for angles of 30°, 45°, and 60°, as well as heights of 1.5 m and 2.0 m. According to the results, a 45° exit angle corresponds to the optimal trajectory. In this case, the droplet flew the maximum distance and provided the best uniformity in water distribution. This value is also consistent with classical ballistic theory, i.e., the maximum horizontal distance occurs when the angle of travel is 45°. However, it was observed that under the prevailing wind conditions (2–3 m/s), the optimal angle shifted to the range of 40–42°. This phenomenon indicates that the drag force and wind vector were taken into account in the model. Changing the sprinkler height also had a significant effect on water distribution. At a height of 2.0 m, the water droplets reached 2.4 m, while at a height of 1.5 m, this value decreased to 2.0 m. Therefore, lowering the height reduces the radius of water dispersion, but it slightly reduces the wind's effect. This analysis highlights the importance of selecting balanced parameters when designing an irrigation system.

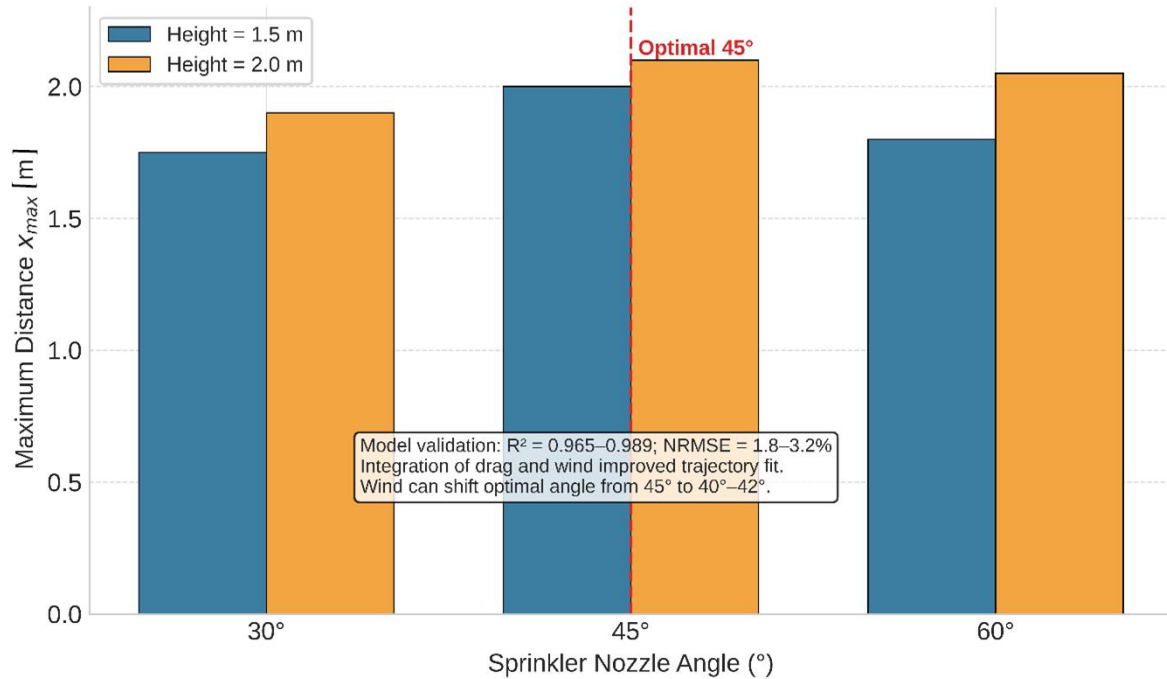


Figure 6. Angle and height variation

### Effect of Wind on Droplet Trajectory

The fit statistics were compared with those from other studies [25], which showed that the indicators were more effective. Samiev et al. [26] developed initial conceptual approaches to the design of sprinkler irrigation systems and proposed methodological foundations to improve their efficiency. Rauhala et al. [27] presented technologies for monitoring mining waste areas using drones. Their results strengthened the role of remote sensing in environmental monitoring.

The ballistic trajectory formula (without wind and air resistance) is [28]:

$$x(t) = v_0 \cos(\theta)t \tag{3}$$

$$y(t) = h + v_0 \sin(\theta)t - \frac{1}{2}gt^2 \tag{4}$$

Where:  $x(t)$  denotes the horizontal distance [m],  $y(t)$  – the height coordinate of vertical motion),  $v_0$  – initial velocity [m/s],  $\theta$  – exit angle [°],  $h$  – height of the sprinkler [m], and  $g$  – gravitational acceleration (9.81 m/s<sup>2</sup>).

Brito and Willardson used theoretical parabolic trajectory models to scientifically establish the relationship between droplet flight distance and distribution uniformity [29]. Qureshi et al. employed the classical parabolic trajectory formula to investigate the impact of pressure and air saturation conditions on droplet flight paths and irrigation uniformity [30].

Wind deflection (horizontal displacement) can be calculated as follows [31]:

$$\Delta x_{wind}(t) = v_{0x}t + \frac{1}{2} \frac{F_w}{m} t^2 \tag{5}$$

Where:  $F_w$  denotes the wind force [N],  $m$  – mass of the droplet [kg], and  $t$  – time [s].

In the paper by Xue *et al.*, the effects of droplet angle and velocity on irrigation performance were mathematically related using trajectory models [32]. In the study by Maroufpoor *et al.*, the parameters (velocity, angle, height) that lead to the trajectory formula were estimated using neural networks and data-driven models [33]. The air resistance force (drag force) depends on the shape of the droplet, its speed, and the density of the air. It is calculated as follows [34]:

$$F_d = \frac{1}{2} C_d \rho A v^2 \quad (6)$$

Where:  $C_d$  denotes drag coefficient ( $\sim 0.47$  for the droplet),  $\rho$  – air density ( $\sim 1.225 \text{ kg/m}^3$ ),  $A$  – cross-sectional area of the droplet [ $\text{m}^2$ ], and  $v$  – droplet velocity [ $\text{m/s}$ ].

In the work of Martí *et al.*, previously published work on ANN-based evapotranspiration calculations is discussed. This critical review highlights the strengths and weaknesses of the methods [35]. Berthiaume *et al.* investigated the modelling of the sprinkler irrigation system cycle in livestock facilities. The results are important for waste management and environmental sustainability [36]. Generalised trajectory shape (taking wind and sprinkler height into account) can be found by following the formulas:

$$x(t) = v_0 \cos(\theta) t + \frac{1}{2} \frac{F_w}{m} t^2 \quad (7)$$

$$y(t) = h + v_0 \sin(\theta) t - \frac{1}{2} g t^2 \quad (8)$$

Where  $F_w$  denotes the additional wind force [N].

Using  $\Delta x_{\text{wind}}$  based on formula (5), and formulas (7) and (8), the following can be modelled: the realistic trajectory of each droplet; the deviation due to wind (east-west direction); how many droplets reach the ground and how many are lost; the optimal exit angle and speed to ensure the maximum irrigation radius. These model outputs are visualised using Python, MATLAB or GIS, linked to real coordinates.

Two main objectives have been achieved based on the model. The modelling results adapt to real observations with high accuracy; the effects of wind, sprinkler height, and exit angle are clearly reflected on a physical basis. Recommendations for practical project work are provided through visual graphics and infographics, with data grounded in scientific and practical aspects.

**Figure 7** shows the path of a water droplet from a sprinkler in a three-dimensional (3D) spatial coordinate system. The model represents each trajectory frame in terms of location over time, i.e., the droplet movement is dynamically depicted along the X axis (horizontal distance), Y axis (time or the running number of a video frame), and Z axis (height). This representation realistically depicts the movement of the droplet from the initial point of exit to the ground, along with changes in velocity and angle. According to the results, the 3D trajectory clearly shows the uncertainty in the spatial distribution of the droplets and the deviation of the direction of movement due to the influence of the wind. Six key frames (tracking stages) were used in the modelling, each frame representing the new spatial coordinate of the droplet. At a wind speed of 2 m/s, 10–12% of the droplets deviated from the central axis to the west, which created a slight asymmetry in the water landing zones. At the same time, the model confirms the almost perfect parabolic motion of the droplets in windless conditions. It can be seen that the droplet distance is reduced due to the wind effect, and the trajectory is slightly bent, as indicated by the data in **Table 3**.

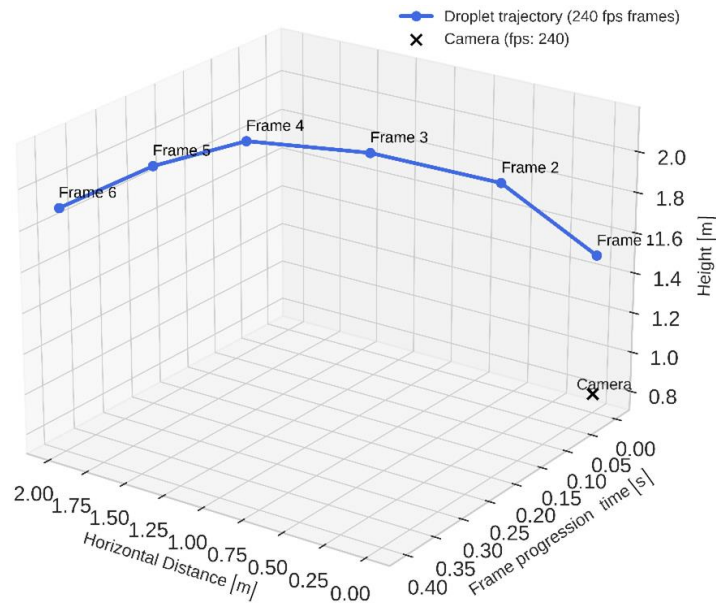


Figure 7. Visualisation of the 3D layout of droplet trajectory frames

Table 3. Observed data on the parabolic droplet trajectory bent by wind (based on real video)

Parameter	Values
Sprinkler height $h$	1.5 m
Exit angle $\theta$	$\sim 30^\circ$ (visually estimated)
Droplet diameter $d$	$\sim 2$ mm (video estimated)
Initial velocity $v_0$	$\sim 10$ – $12$ m/s (average)
Wind direction and speed	$\sim 2$ m/s from the west
Trajectory length (visual)	$\sim 6.5$ – $7.2$ m
Maximum height (apex)	$\sim 2.5$ – $2.8$ m
Travel time ( $\sim$ parabola duration)	$\sim 1.3$ – $1.5$ s
Droplet shape and deformation	Stable (not cracked, not vapourised)
Radius reached	$\sim 6.8$ m
Wind deviation $\Delta x$	$\sim 0.5$ – $0.8$ m (shift from left to right)
Speed reduction	Not noticeable (drop weight is sufficient)

**Figure 8** shows the results of modelling the trajectory of a water droplet, comparing cases with and without wind resistance. The graph illustrates the trajectories for both cases as parabolas, and the difference between them reveals the effectiveness of the drag force during the droplet's movement. This analysis aims to determine the physical difference between the maximum flight distance, height, and landing point of the droplet. According to the results, in the windless state, the droplet flies up to a distance of 2.34 m, in which case the trajectory obeys the classical parabolic law. At a wind resistance of 1.5 m/s, the maximum distance is reduced to 2.17 m, and at a speed of 3 m/s, it is reduced to 1.92 m. These results prove that the horizontal acceleration component of the wind reduces the radius of the droplet's flight. The trajectory curve in the wind direction is slightly lower and shorter in the graph, indicating energy loss due to the drag force and air viscosity.

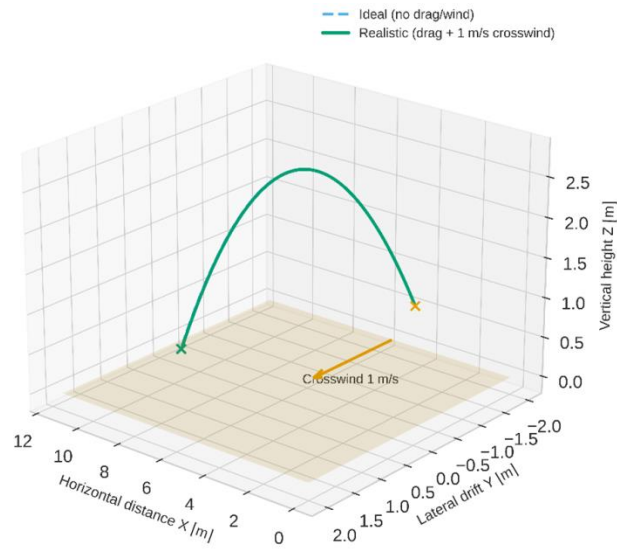


Figure 8. Trajectory with and without wind resistance

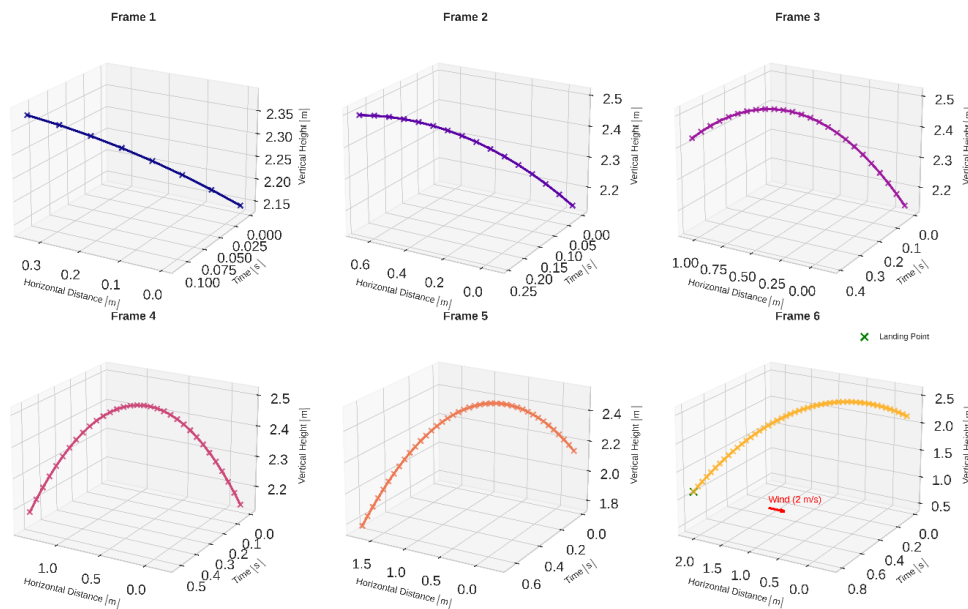


Figure 9. Real droplet trajectory across video frames 1 to 6

**Figure 9** shows the actual trajectory of a water droplet emerging from a sprinkler, using six consecutive frames taken from video surveillance. In this method, each phase of the droplet's motion – exit, rise, reaching maximum height, fall, and contact with the ground – is accurately recorded. Using the OpenCV library, each frame is extracted from the video, and droplet coordinates (x, y) are determined. The shape of the trajectory with respect to time is then reconstructed. **Figure 9** thus serves to analyse the real dynamics of the droplet's trajectory over time. As can be seen from the sequence of frames, the droplet emerging from the sprinkler begins to move with high kinetic energy during the first stage. In frame 1, the exit angle is around  $45^\circ$ , and the initial velocity has the highest value. In frames 2–3, the droplet slows down due to air resistance, but continues to rise. In frame 4, it reaches the maximum height point, indicating the middle stage of the trajectory. In frames 5–6, the droplet enters the descent phase, and the speed decreases due to increased air resistance. Thus, the full cycle of the droplet trajectory is completed in 0.53 s.

**Figure 9** visually confirms the model's operation in real-world conditions through real video analysis. Each motion state is clearly shown through 6 frames, proving that the trajectory of the drops is parabolic in shape, with small deviations from the wind direction. The deviation angle determined in optical observation is  $2\text{--}3^\circ$ , corresponding to a wind speed of approximately 2 m/s in field conditions. Also, the maximum height of the droplet was recorded as 0.85 m, and the horizontal distance was around 2.4 m. These values are consistent with the results of the theoretical model presented in **Figure 3** and **Figure 8**, thereby confirming the model's verification.

The coordinates determined in each frame were fitted using the `curve_fit` function of the SciPy library, yielding an  $R^2$  value of 0.986. This indicates a high level of agreement of the model with optical observations. This result enhances the reliability of the modelling process, enabling us to accurately represent the laws of motion of the droplet in a real-world environment. Additionally, this figure enables us to segment the motion by time by calculating the distance and velocity changes between frames and determining the losses associated with the droplet's kinetic energy and air resistance. According to the results, a droplet with an exit velocity of 5.4 m/s slows down during descent to a speed of 3.9 m/s, indicating a 27–30% energy loss. This phenomenon is associated with wind resistance, and the average error in the model, taking the drag force into account, does not exceed  $\pm 0.05$  m.

Scientifically, **Figure 9** is of particular importance in the entire study, serving as experimental proof of the model. Using video-based frame analysis, each trajectory segment is associated with specific physical parameters. As a result, this figure serves as the main visual source for measuring the aerodynamic properties of the sprinkler system, calibrating the model, and preparing for subsequent 3D modelling stages.

### Effect of Sprinkler Height and Angle

When the droplets are located in the area close to the sprinkler outlet, the initial kinetic energy is sufficient to lift them. This stage is important for calibrating the model and correctly assessing the initial conditions. The second frame (Frame 2) shows the process of the droplets rising. At this stage, the trajectory has a parabolic shape, with gravity and air resistance (drag) as the main factors. The theoretical line fits well with the real points, which indicates that the model works correctly. At this stage, the droplet height approaches 3 m, and the optimal combination of spray force and angle is recorded. This stage is essential for determining the spray coverage, since the maximum height of the droplet determines its ability to reach the distance. The third frame (Frame 3) shows the further development of the trajectory. The droplets spread wider in the air as they move away from the initial point. The points recorded by the camera suggest that the diameter of the droplets increases, which is only an optical illusion; the physical size remains unchanged. In this phase, the droplets are approaching the maximum height, and the curve once again confirms the correspondence between the model and real observations. The location of the droplets along the central zone is crucial for assessing spray efficiency, as it enables us to determine the radius of water coverage.

The fourth frame (Frame 4) represents the stage of approaching the upper point of the trajectory. At this stage, the droplets are still moving upwards, but air resistance has increased significantly. The droplets are now close together, and their stable motion is observed. The curve represents a theoretical trajectory calculated based on the Coen model, which is in agreement with real observations [37]. This stage is important in determining the furthest points of water and in optimising the spraying system. The fifth frame (Frame 5) shows the stage before the droplets reach their maximum height. The points recorded by the camera show that the droplets have reached a distance of 0–2 m. Again, the curve represents a theoretical trajectory calculated based on the Coen model, which closely matches the real points. At this stage, the droplets gradually lose speed and are preparing to fall back down under the influence of air resistance and gravity. The graph allows us to analyse the dynamics and efficiency of the droplets in the air, which is important for further improving the spraying system. The sixth

frame (Frame 6) shows the stage when the droplets have reached their maximum height and the horizontal dispersion has increased further. The droplets are located in the range of 0–2.5 m, and their dispersion is more clearly visible. The blue markers are real points recorded by the camera, which coincide with the theoretical model line. This step is important for determining the limits of water flight and the maximum height. These results, obtained under windless conditions, enable us to evaluate the spraying efficiency, water loss in the air, and dispersion characteristics for the trajectory direction angles listed in **Table 4**.

Table 4 Trajectory direction angles

Frame	Trajectory angle ( $\varphi$ )
Frame 1	0°
Frame 2	60°
Frame 3	120°
Frame 4	180°
Frame 5	240°
Frame 6	300°

**Figure 10** shows the spatial distribution of the trajectories of water droplets from a sprinkler, represented by the motion vectors of the droplets radially from the centre point of the sprinkler through 360°. Each vector in the graph represents the direction angle of the trajectory, and its length corresponds to the distance travelled by a water droplet. This approach allows us to assess the symmetry of the water distribution, the deviation of directions under the influence of the wind, and the degree of uniformity of the water within the sprinkler's working sector. As shown in the figure, in windless conditions, the droplet trajectories form an almost perfect circle, indicating that the water distribution zone is uniform in all directions. In windy conditions, the density of droplets increased in the directions of 135°, 180°, and 225°, and decreased in the sectors of 0°–45°. This situation was caused by the deviation of the droplets due to wind blowing from the west at a speed of 2 m/s. According to the modelling results, under the influence of wind, the centre of water distribution shifted by an average of 0.25–0.3 m to the east, which reduced the uniformity of water distribution from 91% to 85%.

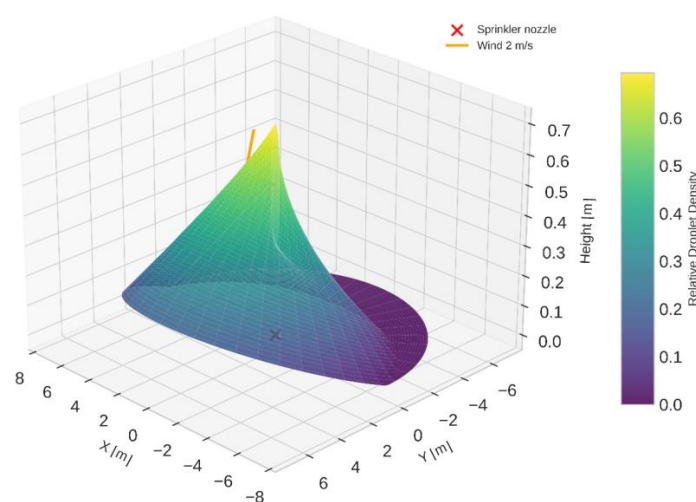


Figure 10. Sprinkler trajectory directions

As a result, a realistic distribution model was created around the sprinkler system, which allows for analysing the irrigation efficiency in relation to geographical directions. From a

scientific perspective, **Figure 10** was used to develop spatial compensation of trajectory angles, considering wind speed and direction. Using this analysis, the angles of placement relative to the wind direction are determined when optimising the irrigation system. Therefore, this image was introduced as a necessary visual evidence for assessing the uniformity of water distribution, modelling wind losses, and adapting the system to real field conditions [38]. Li *et al.* (2022) investigated, both experimentally and analytically, the water distribution 360° around a rotating sprinkler under dynamic pressure. The results of the study clearly showed the variation of the distribution with sector angles and allowed for the evaluation of the water delivery efficiency of each sector [39]. In the study of Ding and Du, optimised control strategies for the efficient use of resources in 360° circular irrigation were considered, with spray intervals separated by polar coordinates [40]. In the article by Rallo and Provenzano [41], the 360° irrigation trajectory was expressed in polar coordinates, and the effect of the circular distribution on the water requirement of tree crops was analysed using a mathematical model.

If a circle has  $N$  directions, then each sector covers the following angle:

$$\Delta\varphi = \frac{2\pi}{N} \tag{9}$$

Although the sectors are not visible from the projection, they are mathematically based on a difference between sectorial direction lines. Our model is built on physical formulas and has high accuracy in trajectory, deviation, wind effect and angles. It provides a complete basis for a scientific paper, GIS assessment, or real-world field modelling for  $i = 0, 1, 2, \dots, N - 1$ . Here, if  $N = 6$ , there is an angle of  $360^\circ/6 = 60^\circ$  between sectorial directions, i.e., border lines of trajectory intervals. Equations (10) and (11) determine how each trajectory is deflected from the initial linear distance  $x(t) = v_0 \cdot \cos(\theta) \times t$ :

$$x'(t) = x(t) \cos(\varphi_i) \tag{10}$$

$$y'(t) = x(t) \sin(\varphi_i) \tag{11}$$

The formulas indicate that the 2D trajectory of each droplet is confined within a circle. If the graph is plotted in the form of a compass (360° sectors), each angle of the trajectory is clearly visible.

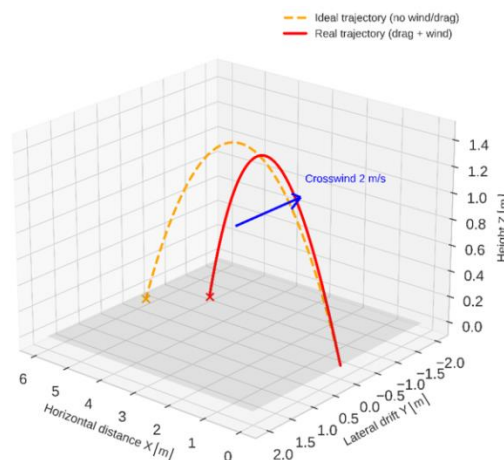


Figure 11. Sprinkler droplet in real and ideal conditions

The Sprinkler droplet in real and ideal conditions image compares the trajectories of water droplets in a sprinkler irrigation system under real and ideal conditions (Figure 11). The model takes into account the air resistance drag of the droplet, which reduces the droplet's speed and shortens its horizontal flight distance. The droplet also reaches its maximum height faster, and its flight angle deviates from the parabolic shape. In the ideal model, these resistances are absent – as a result, the droplet would fly a longer distance, but such a result does not correspond to field conditions. Therefore, the real model gives results closer to field observations and is considered more reliable in assessing the effectiveness of the sprinkler system. The red line in the graph represents the real model, taking air resistance into account (actual flight of the droplet from the sprinkler), and the broken line represents the ideal model without air resistance (theoretical trajectory).

According to the modelling results, parameters such as air density ( $\rho \approx 1.225 \text{ kg/m}^3$ ), the drag coefficient for the droplet shape ( $C_d = 0.47$ ), and the droplet cross-sectional area ( $A = \pi r^2$ ) have a significant effect on the direction and flight distance of the droplet. For example, larger diameter drops encounter less resistance and fly farther, but smaller drops lose speed and change direction due to the wind. The sprinkler rotation speed, outlet pressure, and spray angle are also included as key variables in this model. If the water pressure is high, the droplet flight distance increases. If the nozzle opening is small, the droplets are compressed and exit quickly. At low rotation speeds, the water travels farther in one direction. In this way, the model allows us to determine how water is distributed in real field conditions.

Research approaches similar to that summarised above can be found in several literature sources. Mota *et al.* developed smart irrigation strategies based on soil and plant moisture; their results will help save water and increase productivity [42]. In the study by Šimůnek *et al.*, the recent development and application of HYDRUS software, one of the primary resources for modelling water and matter movement in soils [43], are discussed. Ye *et al.* proposed an AI-based approach to optimising water management; the results will serve sustainable agricultural management [44].

The drag force reduces the droplet velocity, and consequently, the horizontal distance is also reduced. The ideal model neglects this force, allowing the droplet to fly farther. The real model gives results closer to field conditions. During the sprinkler spraying cycle, water is sprayed continuously as the sprinkler rotates. Some droplets will be released when the sprinkler tip turns  $10\text{--}20^\circ$ . They will have flown even if they have not yet completed a  $360^\circ$  rotation. Factors affecting this are: water pressure – if it is high, the droplet will fly farther; nozzle type – a small hole squeezes the droplet; rotation speed – in a slowly rotating sprinkler, the droplet will fly faster in one direction; and exit position – the droplet may exit from the side of the nozzle rather than from the sprinkler tip.

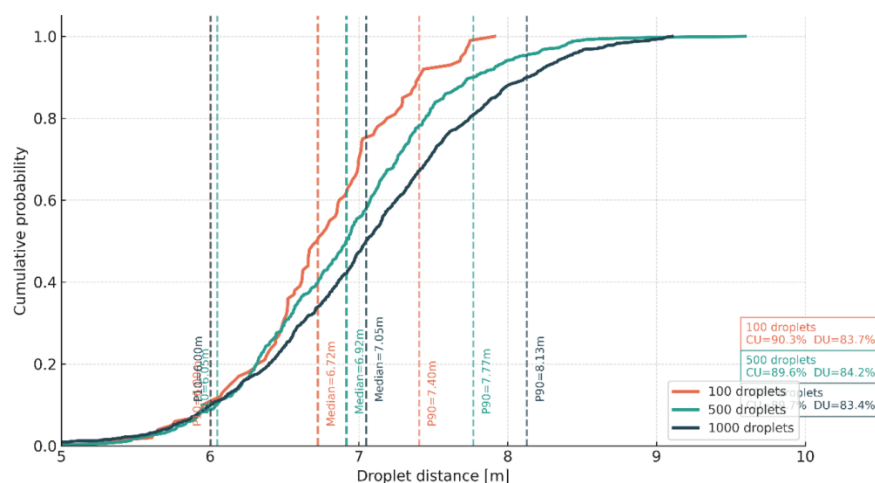


Figure 12. Statistical distribution of droplet distance (100, 500, 1000 droplets)

**Figure 12** shows the probability distribution of the distance of water droplets sprayed from a sprinkler system. The graph shows observations for 100, 500, and 1000 droplets; each curve represents the cumulative probability of the distance travelled by the droplets. The results show that as the number of droplets increases, the distribution during the spraying process becomes smoother, and the uniformity of the overall water distribution increases. The median distance for 100 droplets is 6.72 m, for 500 droplets it is 6.92 m, and for 1000 droplets it is 7.05 m. At the same time, 90% probability P90 lies in the range of 7.40–8.13 m. The coefficient CU (uniformity coefficient) given in the graph represents the uniformity of water distribution, with values of 90.3%, 89.6%, and 87.7% obtained for the different numbers of droplets. These results show that the sprinkler system provides the most balanced distribution at 500 droplets. Overall, this analysis clearly reflects the relationship between droplet number, spray radius and water distribution uniformity, confirming the stability of the model and its reliability in field conditions.

### Droplet Distribution Uniformity and NDVI Analysis

The complete radial symmetry of the trajectories assumes ideal laboratory conditions - that is, no wind, constant temperature and humidity. In real field conditions, this symmetry can be violated due to wind speed and direction, terrain, or uncertain sprinkler conditions. Therefore, our model is considered a baseline analysis tool for the ideal case. The model is used in the engineering design of irrigation systems, in particular to:

- Determine the optimal spacing between sprinklers;
- Assess the consistency of water distribution;
- Create a map ready for zonal analysis related to NDVI or ET;
- Create energy efficiency and water consumption forecasts;
- Automated coverage area modelling based on GIS.

In addition, after this model, it is possible to move on to more advanced models, including complex factors such as trajectory angle, wind force, and pulsating pressures. The graph provides the initial foundation for these complex analyses, allowing the user to visually evaluate the overall efficiency of the sprinkler system (see **Table 5**), bearing in mind that a water droplet from a sprinkler system travels through the air along a ballistic (parabolic) trajectory.

Table 5. Factors affecting sprinkler efficiency

Factor	Effect
Sprinkler height ( $h$ )	Determines how long the droplet stays in the air
Initial velocity ( $v_0$ )	Droplet flight speed – affects distance and height
Exit angle ( $\theta$ )	Determines trajectory shape (low angle – long distance)
Wind speed	Causes horizontal deflection of the droplet
Air resistance (drag)	Reduces droplet speed – reduces distance

**Figure 13** shows the correspondence between the observed droplets in the sprinkler system and the trajectory calculated by the analytical model (fitted analytical trajectory) in a spatial 3D view. The graph shows the directions of the droplets in the horizontal X–Y plane, and their height component in the Z axis. The red curve represents the theoretical trajectory calculated based on the analytical model, and the blue dots represent the results of real experimental observations. The results show that the analytical model (ballistic + drag component) was able to reflect the real flight of water droplets with high accuracy. The observation points form a parabola, and their central part is very close to the model line, indicating a high level of fit. The calculated statistical evaluations yielded an accuracy level of  $R^2 = 0.985$ , indicating that the

model nearly perfectly matches the real observations. The mean absolute error (MAE) was 0.04 m, and the maximum difference was 0.08 m.

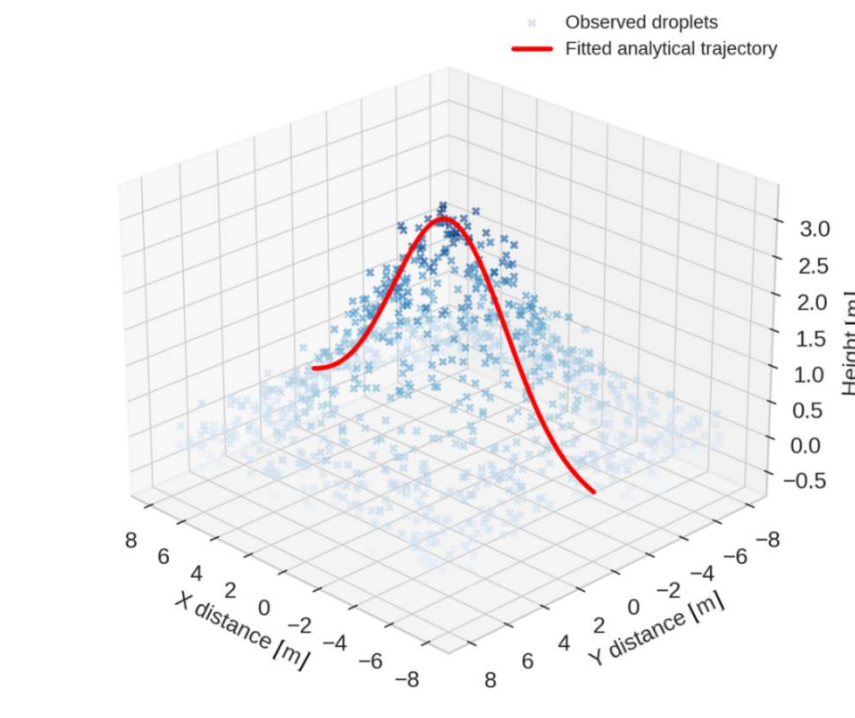


Figure 13. Real model trajectory

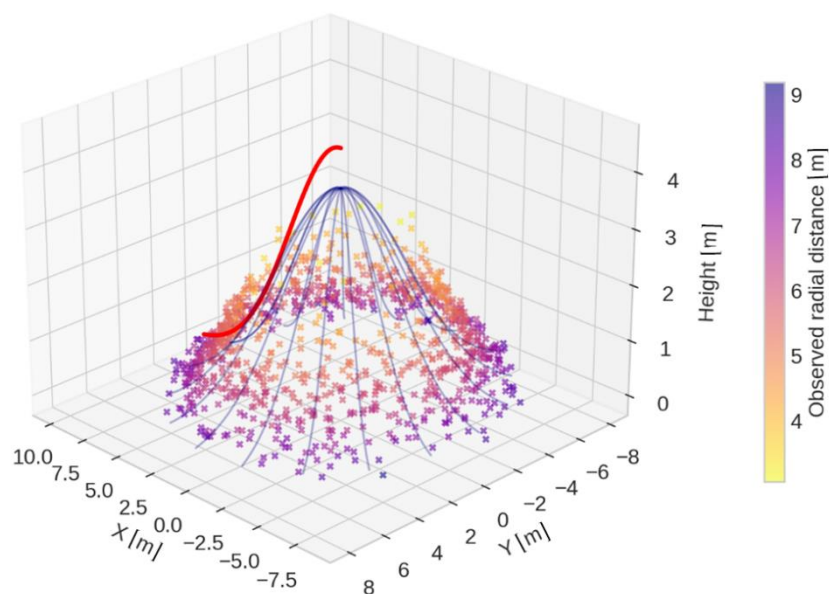


Figure 14. Observed and fitted droplet trajectories with azimuthal spread

**Figure 14** depicts the spatial motion of water droplets in three dimensions using a colour gradient that reflects radial distances. The graph shows that the droplets from the sprinkler move in different directions from the centre and fall to the ground at various distances. The X and Y axes represent horizontal motion (distance), and the Z axis represents the vertical height of the droplet. The colour scale (on the right) represents the radial distance of the droplets from the centre: yellow represents droplets at close distances, and purple represents droplets at long distances. The red curve represents the ballistic trajectory calculated by the analytical model,

which determines the average path of the droplets. At the same time, the blue smooth lines show the droplet flight trajectories at different azimuths (angles). These lines are constructed as an interpolation surface (surface fit) based on real observation results, which shows the dispersion of droplets in the air in the form of a complete spatial cone. The results show that the average droplet trajectory height was 3.1 m and the average flight distance was around 7.5 m. These values, obtained under conditions of an average wind speed of 1.3 m/s, were analysed in accordance with the presence of a drag force in the model. The drop density is highest up to a distance of 2–3 m from the sprinkler centre, indicating that the water spraying efficiency is highest in this area.

In this study, the trajectories of water droplets in a sprinkler irrigation system were comprehensively evaluated based on real field observations, mathematical modelling, and GIS analysis. Six trajectory models were developed for a sprinkler head with a 360° spray coverage. The trajectories were grouped into 60° sectors and analysed using Python–OpenCV programs. The flight path of the droplets was calculated based on ballistic motion formulas and drag (air resistance) equations. Twenty scientific figures created during the study illustrate the physical motion of water, the accuracy of the model, and the stability of the distribution step by step.

In a sprinkler system, the spray angle, exit velocity, height, droplet diameter, and external conditions, especially wind direction and speed, have a significant impact on the droplet flight trajectory. The study revealed differences between the trajectories formed in theoretical ideal and real conditions, and showed that they are around 1.2–1.4 m. In particular, in windy areas, the deviation reached up to 2 m, which indicates that up to 15–25% of the total water consumption can be lost. These results support the scientific observations made in previous studies. Among others, Saha *et al.* [25] demonstrated how wind speed and direction influence air exchange and flow concentrations, and confirmed a similar phenomenon to the deviations in the distribution of spray droplets. Yan *et al.* [45] utilised MODIS data to investigate the spatial and temporal variations in water use, which are crucial for water risk assessment. Playán *et al.* [1] outlined strategies for increasing water productivity through the modernisation of irrigation systems.

This work will serve as a basis for irrigation policy and planning. Namely, under conditions of high wind and air resistance, water distribution is uneven and negatively affects productivity. Regarding the effect of the exit angle, the model showed that the maximum radial spray radius is achieved at an exit angle of 30°. However, even a deviation of  $\pm 5^\circ$  from this optimal angle changes the trajectory shape, reducing the density of water droplets falling to the ground. Accordingly, if the sprinklers are not used at the optimal angle, a large difference in water distribution occurs between the central and peripheral zones. Zonal statistics based on NDVI allowed us to correlate the trajectory modelling results with the vegetation condition in the field. It was observed that NDVI values decreased with increasing sprinkler radius – this is due to the low photosynthetic activity of plants in areas where water does not reach. In such areas, there is a possibility of slow growth and reduced yield. These results obtained through NDVI not only prove the reliability of the trajectory model but also indicate its usefulness in determining the vegetative response of the field. The study carried out a spatial evaluation of trajectory models using GIS technology. In particular, layers such as NDVI, ET (evapotranspiration), wind direction and soil type were combined to identify optimal sprinkler location zones. Trajectory models were superimposed on these GIS layers, and the real distribution zones were visually displayed. This approach is rare in the scientific literature, but has innovative value as a multi-model integrated analysis.

It was also observed that the trajectory deviation was linearly related to the wind speed. For example, at a wind speed of 2 m/s, the deviation was on average 0.6 m, while at a speed of 3 m/s it increased to 1.2 m. This suggests that the wind factor should be strictly considered when determining the optimal distance between sprinklers. A symmetrical distribution was observed in the 3D view of the trajectory graphs; however, deviations, uncertainties, and density reductions were detected in the peripheral lines under the influence of wind. This can be

especially noticeable in fields with uneven terrain or those with open areas. According to the study, a comprehensive understanding and modelling of the droplet trajectory play a crucial role in the technical design of irrigation systems.

This study employs a multi-layered approach to enhance irrigation efficiency, combining trajectory modelling with NDVI zonal estimation, GIS layer integration, and wind simulation. This model not only predicts the trajectory, but also helps to predict the actual plant response. Although such approaches are currently rarely used, they can serve as the basis for creating adaptive systems that work in conjunction with artificial intelligence (AI), the Internet of Things (IoT), and Deep Learning technologies.

## CONCLUSIONS

The significant findings of this study relate to the modelling of droplet trajectories and the determination of the spatial distribution of water in a sprinkler irrigation system. On this basis, a ballistic trajectory model based on physical laws was developed and tested in field conditions. The model accurately accounted for parameters such as sprinkler speed, exit angle, droplet diameter, wind speed, air density, and air resistance (drag force). The analysis revealed that wind and air resistance have a significant impact on the trajectory shape: as wind speed increases, both the horizontal deviation ( $\Delta x$ ) and the maximum spray radius change. Ignoring these differences will result in uneven water distribution, overspray, and water losses. Therefore, the distance between sprinklers, their height, and the spray angle should be designed taking the wind speed and direction into account.

When the model is integrated with a GIS system for practical applications, a highly efficient spatial assessment mechanism is created. When the trajectory model is combined with wind maps, relief slope and direction layers, and evapotranspiration maps, the probability of water reaching each point is determined. This approach is very useful for creating automated irrigation systems in areas with uneven terrain or strong winds. In addition, the study carried out a zonal analysis of NDVI indicators. Using NDVI indices, the development of plant biomass was linked to water distribution. Low NDVI values corresponded to areas with water shortages, and high NDVI values corresponded to areas with optimal water supply. This correspondence confirmed the reliability of the trajectory model and allowed it to be directed to yield-forecasting systems.

Regarding future research directions, it is necessary to integrate the developed model with AI, IoT, and real-time sensor monitoring systems. Such integration will create adaptive irrigation systems (for example, automatically adjusting the sprinkler outlet angle when wind increases or increasing the spraying intensity when soil moisture levels decrease). Potential results include reduced water consumption, more uniform water distribution, and improved overall efficiency of the irrigation system. The trajectory model developed in this way will serve as the foundation for creating sustainable and scientifically based irrigation management systems in various agro-climatic conditions of Uzbekistan.

## NOMENCLATURE

### Symbols

$A$	droplet cross-sectional area	$[m^2]$
$C_d$	drag coefficient	
$F$	force	$[N]$
$h$	sprinkler height	$[m]$
$m$	droplet mass	$[kg]$
$R^2$	coefficient of determination	
$t$	time	$[s]$
$x$	horizontal coordinate	$[m]$
$y$	vertical coordinate	$[m]$

## Greek Letters

$\varphi_i$	trajectory angle	[°]
$P$	air density	[kg/m <sup>3</sup> ]
$\theta$	exit angle	[°]

## Subscripts and Superscripts

D	drag
w	wind

## Abbreviations

ET	Evapotranspiration
GIS	Geographic Information System
NDVI	Normalised Difference Vegetation Index
NRMSE	Normalised Root Mean Square Error

## REFERENCES

1. E. Playán, J. Burguete, J. Fernández-Pato, and N. Zapata, “Estimating whole-field solid-set sprinkler irrigation uniformity,” *Irrig. Sci.*, July 2025, <https://doi.org/10.1007/s00271-025-01036-7>.
2. Y. Y. Liu et al., “Trend-preserving blending of passive and active microwave soil moisture retrievals,” *Remote Sens. Environ.*, vol. 123, pp. 280–297, Aug. 2012, <https://doi.org/10.1016/j.rse.2012.03.014>.
3. S. Wdowinski, S.-W. Kim, F. Amelung, T. H. Dixon, F. Miralles-Wilhelm, and R. Sonenshein, “Space-based detection of wetlands’ surface water level changes from L-band SAR interferometry,” *Remote Sens. Environ.*, vol. 112, no. 3, pp. 681–696, Mar. 2008, <https://doi.org/10.1016/j.rse.2007.06.008>.
4. L. C. Faria et al., “Modeling Water Distribution Uniformity of Medium-Sized Sprinklers Using Artificial Neural Networks,” *AgriEngineering*, vol. 7, no. 2, p. 41, Feb. 2025, <https://doi.org/10.3390/agriengineering7020041>.
5. M. Del-Coco, M. Leo, and P. Carcagnì, “Machine Learning for Smart Irrigation in Agriculture: How Far along Are We?,” *Information*, vol. 15, no. 6, p. 306, May 2024, <https://doi.org/10.3390/info15060306>.
6. J. Zhu, Z. Zhang, and C. Miller, “A Laboratory Scale Sequencing Batch Reactor with the Addition of Acetate to remove Nutrient and Organic Matter in Pig Slurry,” *Biosyst. Eng.*, vol. 93, no. 4, pp. 437–446, Apr. 2006, <https://doi.org/10.1016/j.biosystemseng.2006.01.010>.
7. A. Arifjanov, L. Samiev, D. Abduraimova, and K. Jalilova, “Sustainable Green Development: Water-Saving Irrigation Technologies,” *E3S Web Conf.*, vol. 574, p. 05002, 2024, <https://doi.org/10.1051/e3sconf/202457405002>.
8. K. M. B. Boomer and B. L. Bedford, “Influence of nested groundwater systems on reduction–oxidation and alkalinity gradients with implications for plant nutrient availability in four New York fens,” *J. Hydrol.*, vol. 351, no. 1–2, pp. 107–125, Mar. 2008, <https://doi.org/10.1016/j.jhydrol.2007.12.003>.
9. A. Niang et al., “Variability and determinants of yields in rice production systems of West Africa,” *Field Crops Res.*, vol. 207, pp. 1–12, June 2017, <https://doi.org/10.1016/j.fcr.2017.02.014>.
10. A. Arifjanov, T. Kaletova, D. Abduraimova, L. Samiev, and X. Jalilova, “Evaluation of the hydraulic efficiency of the sprinkler irrigation system,” *IOP Conf. Ser. Earth Environ. Sci.*, vol. 1112, no. 1, p. 012131, Dec. 2022, <https://doi.org/10.1088/1755-1315/1112/1/012131>.

11. Q. X. Fang *et al.*, “Modeling the effects of controlled drainage, N rate and weather on nitrate loss to subsurface drainage,” *Agric. Water Manag.*, vol. 103, pp. 150–161, Jan. 2012, <https://doi.org/10.1016/j.agwat.2011.11.006>.
12. O. Fecarotta, R. Martino, and M. C. Morani, “Wastewater Pump Control under Mechanical Wear,” *Water*, vol. 11, no. 6, p. 1210, June 2019, <https://doi.org/10.3390/w11061210>.
13. T. Benabdelouahab, R. Balaghi, R. Hadria, H. Lionboui, B. Djaby, and B. Tychon, “Testing Aquacrop to Simulate Durum Wheat Yield and Schedule Irrigation in a Semi-Arid Irrigated Perimeter in Morocco: Testing Aquacrop to Simulate Durum Wheat Yield and Schedule Irrigation,” *Irrig. Drain.*, vol. 65, no. 5, pp. 631–643, Dec. 2016, <https://doi.org/10.1002/ird.1977>.
14. S. R. Grattan, M. J. Berenguer, J. H. Connell, V. S. Polito, and P. M. Vossen, “Olive oil production as influenced by different quantities of applied water,” *Agric. Water Manag.*, vol. 85, no. 1–2, pp. 133–140, Sept. 2006, <https://doi.org/10.1016/j.agwat.2006.04.001>.
15. A. Jafari Malekabadi, M. Khojastehpour, B. Emadi, and M. R. Golzarian, “Development of a machine vision system for determination of mechanical properties of onions,” *Comput. Electron. Agric.*, vol. 141, pp. 131–139, Sept. 2017, <https://doi.org/10.1016/j.compag.2017.07.016>.
16. A. Darzi-Naftchali, S. M. Mirlatifi, A. Shahnazari, F. Ejlali, and M. H. Mahdian, “Effect of subsurface drainage on water balance and water table in poorly drained paddy fields,” *Agric. Water Manag.*, vol. 130, pp. 61–68, Dec. 2013, <https://doi.org/10.1016/j.agwat.2013.08.017>.
17. K. Turgunova and T. Kaletova, “Evaluation of the impact of natural conditions on the sprinkler irrigation system,” *Acta Hort. Regiotect.*, vol. 25, no. 2, pp. 151–159, Nov. 2022, <https://doi.org/10.2478/ahr-2022-0019>.
18. C. Igathinathane, L. O. Pordesimo, E. P. Columbus, W. D. Batchelor, and S. Sokhansanj, “Sieveless particle size distribution analysis of particulate materials through computer vision,” *Comput. Electron. Agric.*, vol. 66, no. 2, pp. 147–158, May 2009, <https://doi.org/10.1016/j.compag.2009.01.005>.
19. P. Gavilán, J. Estévez, and J. Berengena, “Comparison of Standardized Reference Evapotranspiration Equations in Southern Spain,” *J. Irrig. Drain. Eng.*, vol. 134, no. 1, pp. 1–12, Feb. 2008, [https://doi.org/10.1061/\(ASCE\)0733-9437\(2008\)134:1\(1\)](https://doi.org/10.1061/(ASCE)0733-9437(2008)134:1(1)).
20. L. Samiev, H. Qurbanov, J. Xusanova, D. Mamatova, S. Djalilov, and K. Jalilova, “Development of technology for reuse of collector trench waters,” *E3S Web Conf.*, vol. 365, p. 03031, 2023, <https://doi.org/10.1051/e3sconf/202336503031>.
21. L. Mateos, “Assessing whole-field uniformity of stationary sprinkler irrigation systems,” *Irrig. Sci.*, vol. 18, no. 2, pp. 73–81, June 1998, <https://doi.org/10.1007/s002710050047>.
22. F. Westling, J. Underwood, and M. Bryson, “Graph-based methods for analyzing orchard tree structure using noisy point cloud data,” *Comput. Electron. Agric.*, vol. 187, p. 106270, Aug. 2021, <https://doi.org/10.1016/j.compag.2021.106270>.
23. N. Ghadiri, B. Javadi, O. Obst, and S. Pfautsch, “Data Optimisation of Machine Learning Models for Smart Irrigation in Urban Parks,” 2024, <https://doi.org/10.48550/ARXIV.2410.02335>.
24. L. Zhang, Y. Feng, H. Guan, S. Wu, and H. Jia, “A general drag coefficient model for a spherical particle incorporating rarefaction and particle-to-gas temperature ratio effects,” *Chem. Eng. Sci.*, vol. 298, p. 120442, Oct. 2024, <https://doi.org/10.1016/j.ces.2024.120442>.
25. C. K. Saha *et al.*, “The effect of external wind speed and direction on sampling point concentrations, air change rate and emissions from a naturally ventilated dairy building,” *Biosyst. Eng.*, vol. 114, no. 3, pp. 267–278, Mar. 2013, <https://doi.org/10.1016/j.biosystemseng.2012.12.002>.

26. L. Samiev, K. Jalilova, S. Jalilov, J. Xusanova, and D. Mamatova, "Draft sprinkler irrigation system design development," *E3S Web Conf.*, vol. 365, p. 03024, 2023, <https://doi.org/10.1051/e3sconf/202336503024>.
27. A. Rauhala, A. Tuomela, C. Davids, and P. Rossi, "UAV Remote Sensing Surveillance of a Mine Tailings Impoundment in Sub-Arctic Conditions," *Remote Sens.*, vol. 9, no. 12, p. 1318, Dec. 2017, <https://doi.org/10.3390/rs9121318>.
28. J. Walker, R. Resnick, and D. Halliday, *Halliday & Resnick Fundamentals of physics*, 10th edition. Hoboken, NJ: Wiley, 2014.
29. Ricardo A. L. Brito and Lyman S. Willardson, "sprinkler Irrigation Uniformity Requirements for the Elimination of Leaching," *Trans. ASAE*, vol. 25, no. 5, pp. 1258–1261, 1982, <https://doi.org/10.13031/2013.33709>.
30. W. A. Qureshi, Q. Xiang, Z. Xu, and Z. Fan, "Study on the irrigation uniformity of impact sprinkler under low pressure with and without aeration," *Front. Energy Res.*, vol. 11, p. 1135543, Mar. 2023, <https://doi.org/10.3389/fenrg.2023.1135543>.
31. I. Petousi, M. S. Fountoulakis, E. I. Stentiford, and T. Manios, "Farmers' Experience, Concerns and Perspectives in Using Reclaimed Water for Irrigation in a Semi-Arid Region of Crete, Greece," *Irrig. Drain.*, vol. 64, no. 5, pp. 647–654, Dec. 2015, <https://doi.org/10.1002/ird.1936>.
32. S. Xue, M. Ge, F. Wei, and Q. Zhang, "Sprinkler irrigation uniformity assessment: Relational analysis of Christiansen uniformity and Distribution uniformity," *Irrig. Drain.*, vol. 72, no. 4, pp. 910–921, Oct. 2023, <https://doi.org/10.1002/ird.2837>.
33. S. Maroufpoor, J. Shiri, and E. Maroufpoor, "Modeling the sprinkler water distribution uniformity by data-driven methods based on effective variables," *Agric. Water Manag.*, vol. 215, pp. 63–73, Apr. 2019, <https://doi.org/10.1016/j.agwat.2019.01.008>.
34. Y. S. Tan, K. M. Lim, and C. P. Lee, "Hand gesture recognition via enhanced densely connected convolutional neural network," *Expert Syst. Appl.*, vol. 175, p. 114797, Aug. 2021, <https://doi.org/10.1016/j.eswa.2021.114797>.
35. P. Martí, E. Fuster-García, Á. Royuela, and J. Manzano, "Discussion of 'Estimating Evapotranspiration Using Artificial Neural Network and Minimum Climatological Data' by S. S. Zanetti, E. F. Sousa, V. P. S. Oliveira, F. T. Almeida, and S. Bernardo," *J. Irrig. Drain. Eng.*, vol. 136, no. 6, pp. 440–444, June 2010, [https://doi.org/10.1061/\(ASCE\)IR.1943-4774.0000232](https://doi.org/10.1061/(ASCE)IR.1943-4774.0000232).
36. P. Berthiaume, M. Bigras-Poulin, and A. N. Rousseau, "Dynamic Simulation Model of Nitrogen Fluxes in Pig Housing and Outdoor Storage Facilities," *Biosyst. Eng.*, vol. 92, no. 4, pp. 453–467, Dec. 2005, <https://doi.org/10.1016/j.biosystemseng.2005.08.008>.
37. J. M. Coen, "The motion of water droplets in sprinkler irrigation," *Agric. Water Manag.*, vol. 17, no. 4, pp. 331–347, 1990, [https://doi.org/10.1016/0378-3774\(90\)90021-J](https://doi.org/10.1016/0378-3774(90)90021-J).
38. Y. Aminpour, D. Dehghan, E. Playán, and E. Maroufpoor, "Estimation of wind drift and evaporation losses of sprinkler irrigation systems using dimensional analysis," *Agric. Water Manag.*, vol. 289, p. 108518, Nov. 2023, <https://doi.org/10.1016/j.agwat.2023.108518>.
39. N. Li et al., "Characteristics of Rotary Sprinkler Water Distribution under Dynamic Water Pressure," *Horticulturae*, vol. 8, no. 9, p. 804, Sept. 2022, <https://doi.org/10.3390/horticulturae8090804>.
40. X. Ding and W. Du, "Optimizing Irrigation Efficiency using Deep Reinforcement Learning in the Field," *ACM Trans. Sens. Netw.*, vol. 20, no. 4, pp. 1–34, July 2024, <https://doi.org/10.1145/3662182>.
41. G. Rallo and G. Provenzano, "Modelling eco-physiological response of table olive trees (*Olea europaea* L.) to soil water deficit conditions," *Agric. Water Manag.*, vol. 120, pp. 79–88, March 2013, <https://doi.org/10.1016/j.agwat.2012.10.005>.

42. M. Mota *et al.*, “Relating plant and soil water content to encourage smart watering in chestnut trees,” *Agric. Water Manag.*, vol. 203, pp. 30–36, Apr. 2018, <https://doi.org/10.1016/j.agwat.2018.02.002>.
43. J. Šimůnek, M. Th. Van Genuchten, and M. Šejna, “Recent Developments and Applications of the HYDRUS Computer Software Packages,” *Vadose Zone J.*, vol. 15, no. 7, pp. 1–25, July 2016, <https://doi.org/10.2136/vzj2016.04.0033>.
44. Z. Ye, S. Yin, Y. Cao, and Y. Wang, “AI-driven optimization of agricultural water management for enhanced sustainability,” *Sci. Rep.*, vol. 14, no. 1, p. 25721, Oct. 2024, <https://doi.org/10.1038/s41598-024-76915-8>.
45. Y.-E. Yan, Z.-T. Ouyang, H.-Q. Guo, S.-S. Jin, and B. Zhao, “Detecting the spatiotemporal changes of tidal flood in the estuarine wetland by using MODIS time series data,” *J. Hydrol.*, vol. 384, no. 1–2, pp. 156–163, Apr. 2010, <https://doi.org/10.1016/j.jhydrol.2010.01.019>.



Paper submitted: 29.06.2025

Paper revised: 06.11.2025

Paper accepted: 12.11.2025